Electronic Supporting Information (ESI) for

Tartaric acid regulated the advanced synthesis of bismuth-based materials with tunable performance towards the electrocatalytic production of hydrogen peroxide

Paul Morandi,[1] Valerie Flaud,[2] Sophie Tingry,[1] David Cornu,[1] and Yaovi Holade[1,*]

[1]Institut Européen des Membranes, IEM UMR 5635, Univ Montpellier, ENSCM, CNRS, Montpellier, France.

[2]Institut Charles Gerhardt, ICGM UMR 5253, Univ Montpellier, ENSCM, CNRS, Montpellier, France

Corresponding Author:
*Y.H.: E-mail: yaovi.holade@enscm.fr

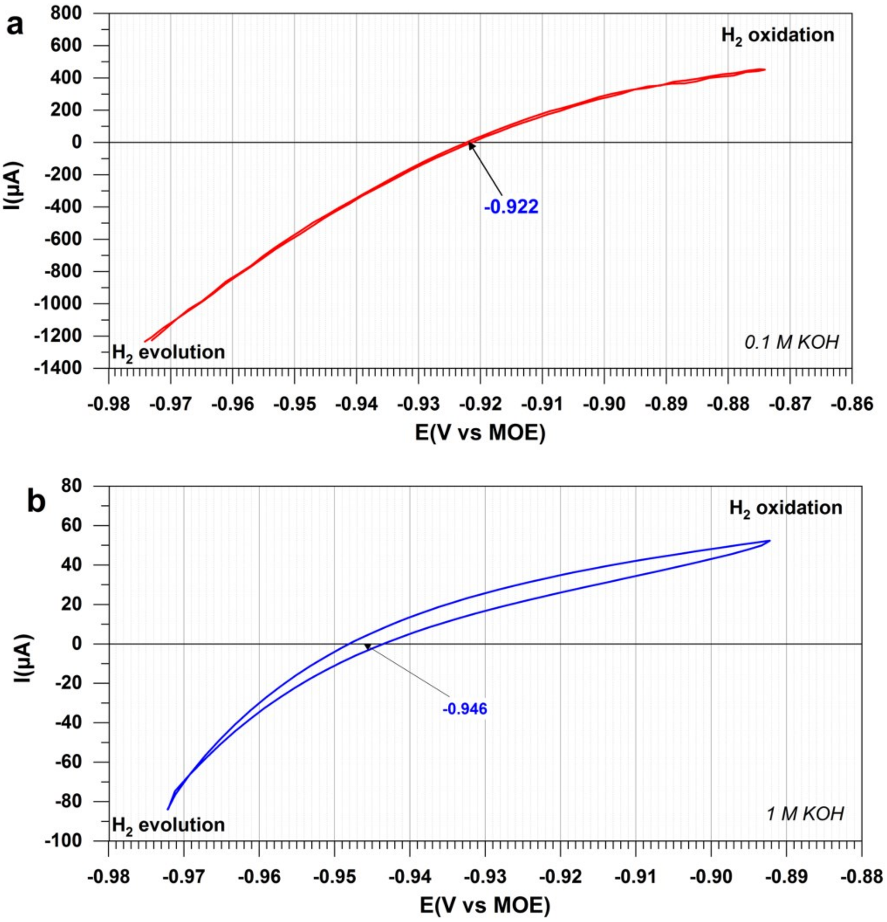

Fig. S1. CV experiment for the calibration of the reference electrode. Steady-state CV recorded in H_2-saturated electrolyte at 1 mV s^{-1} at 25 °C by employing a Pt plate as the working electrode, a Pt mesh as the counter electrode and a Hg|HgO|KOH filled with 0.1 or 1 M as the reference electrode, referred to as MOE. (a) Experiment in 0.1 M KOH (stirred). (b) Experiments in a quiescent solution of 1 M KOH.

Comment: The average of the two potentials at which the current crossed zero is taken to be the thermodynamic potential for the hydrogen electrode reactions. Thus, the scaling relationship is as following:

For 0.1 M KOH: E(V vs RHE) = E(V vs MOE) + 0.922

For 1 M KOH: E(V vs RHE) = E(V vs MOE) + 0.946

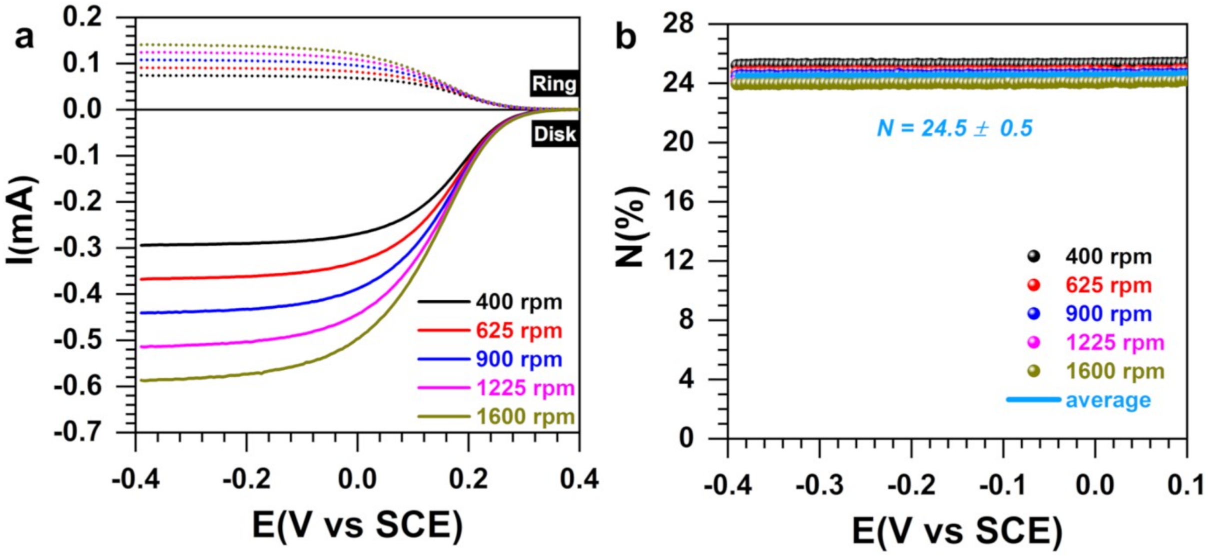

Fig. S2. Determination of the collection efficiency of the RRDE setup. (a) LSV recorded at different speeds in N_2-saturated 1 M KNO_3 electrolyte in the presence of 5 mM $K_3[Fe(CN)_6]$ at 5 mV s^{-1} and room temperature. (b) The corresponding collection efficiency (N), the average is 24.5 ± 0.5%, in agreement with the manufacturer's value of 24.9%.

Comment:

- Basics: The collection efficiency (N) of a RRDE is defined as the fraction of the species formed at the disk that arrive at the ring and react there.[1,2] The value is specific to the geometry of the RRDE, i.e., does not depend on the studied redox reaction. The simple and elegant way to experimentally evaluate N consists of considering a simple reduction reaction, the most routine one being $[Fe^{(III)}(CN)_6]_3^- + e^- = [Fe^{(II)}(CN)_6]_4^-$. To make this effective, the potential at which the ring should be held must be higher than the potential where the produced intermediate at the disk is expected to react electrochemically, which is typically the reverse of the process undergoing at the disk. For the Fe(III)/Fe(II), this is usually chosen higher than 0.77 V vs SHE for $E°(Fe^{3+}/Fe^{2+})$. For ORR, the ring should be fixed at 1.1-1.3V vs RHE (E_{RHE} vs E_{SHE} = -0.059pH at 25 °C) to be able to oxidize H_2O_2 or HO_2^- intermediates ($pKa(H_2O_2/HO_2^-) = 11.75$). To these ends, a four-electrode potentiostat needs to be implemented. In this configuration, both potentials of the disk and the ring are controlled with respect to the reference electrode independently. Hence, their corresponding current is measured separately.
- Application to Fig. S2. Starting from the higher potential (Fig. S2a), the ferricyanide (Fe^{III}) is reduced at the disk (GC), and the generated ferrocyanide (Fe^{II}) is "radially" swept outward away from the disk toward the ring (Pt). Finally, only a fraction of those Fe^{II} species reaches the ring where they undergo an oxidation back to Fe^{III}. Fig. S2a shows the calculated value from Eq. S1, where I_R and I_D represent the current of the ring and the disk, respectively. Please note that the relationship is not valid for the current densities.

$$N = -\frac{I_R}{I_D} = \frac{I_R}{|I_D|} \leq 1 \qquad \text{Eq. S1}$$

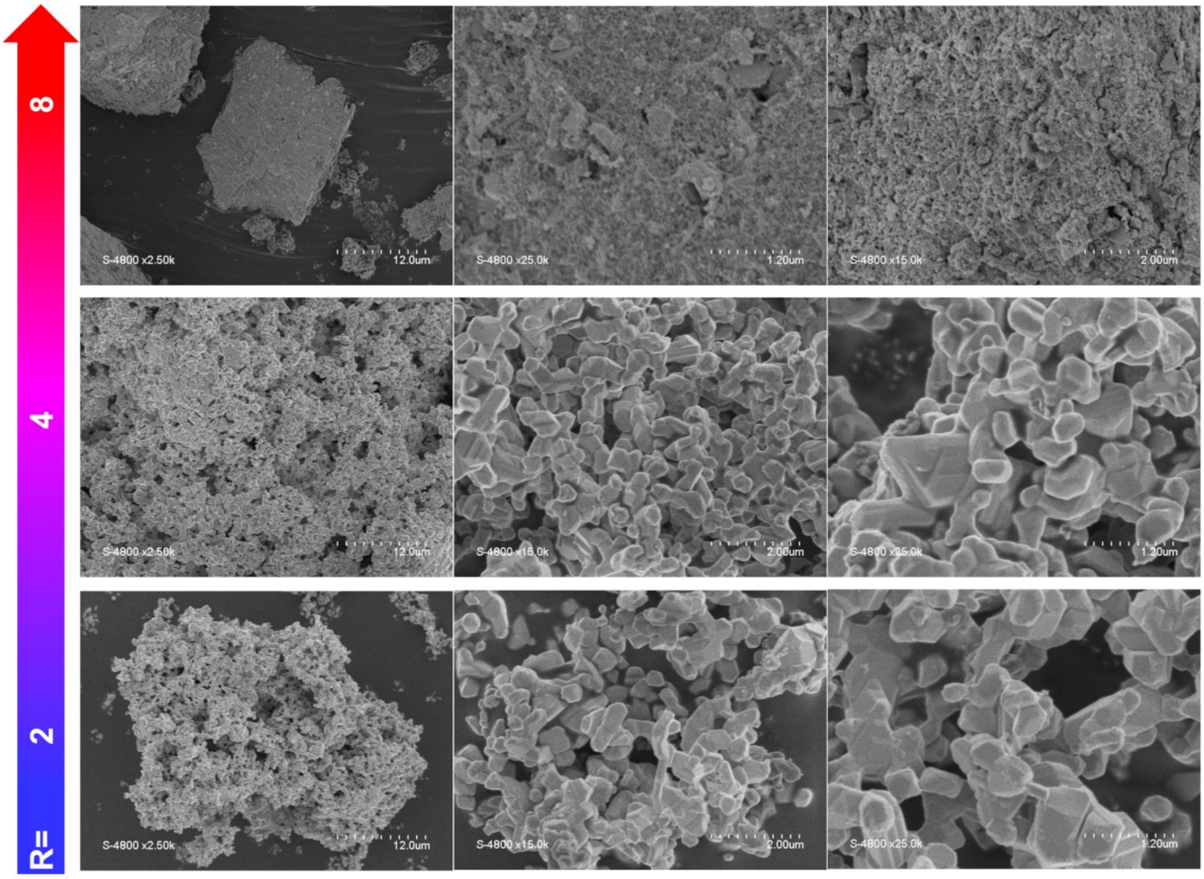

Fig. S3. From bottom to up: SEM images of the as-synthesized bismuth-based materials for ratio $R = n(\mathrm{NaOH})/n(\mathrm{Bi(NO_3)_3 \cdot 5H_2O}) = 2$, 4 and 8. Left to right: from an overview to a closer-view.

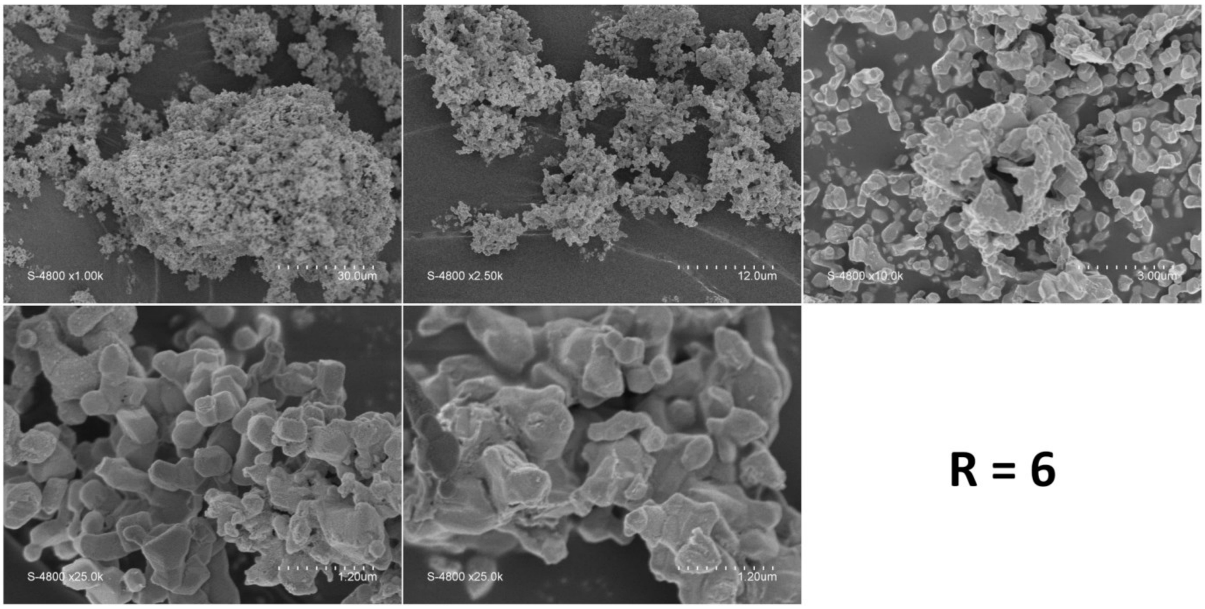

Fig. S4. SEM images of the as-synthesized bismuth-based material for ratio $R = n(\mathrm{NaOH})/n(\mathrm{Bi(NO_3)_3 \cdot 5H_2O}) = 6$.

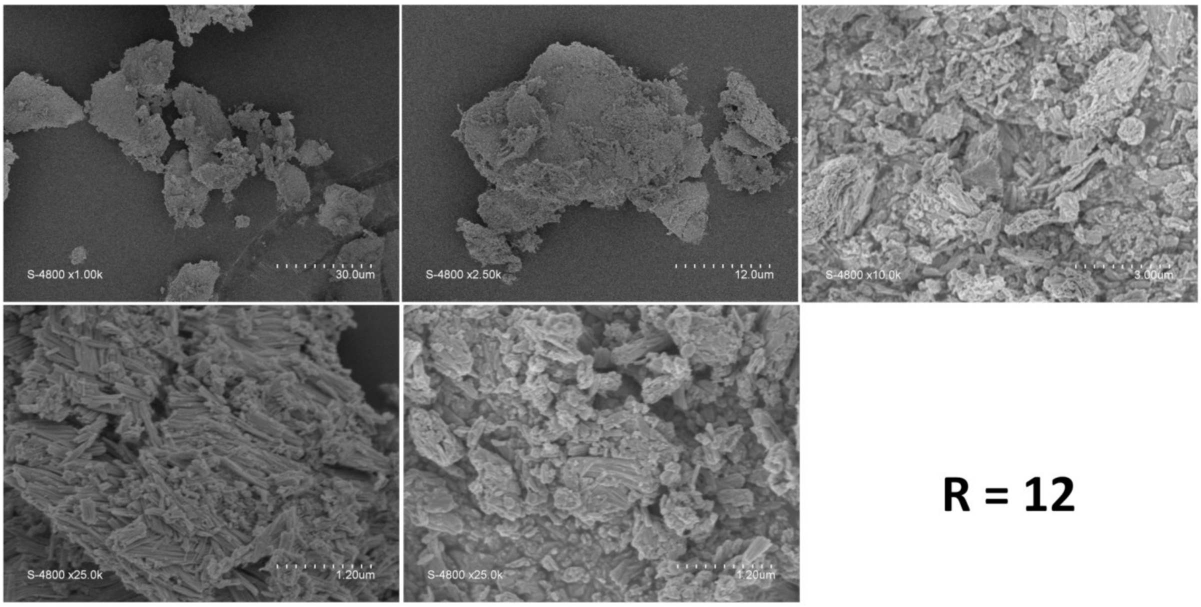

Fig. S5. SEM images of the as-synthesized bismuth-based material for ratio $R = n(\mathrm{NaOH})/n(\mathrm{Bi(NO_3)_3{\cdot}5H_2O}) = 12$.

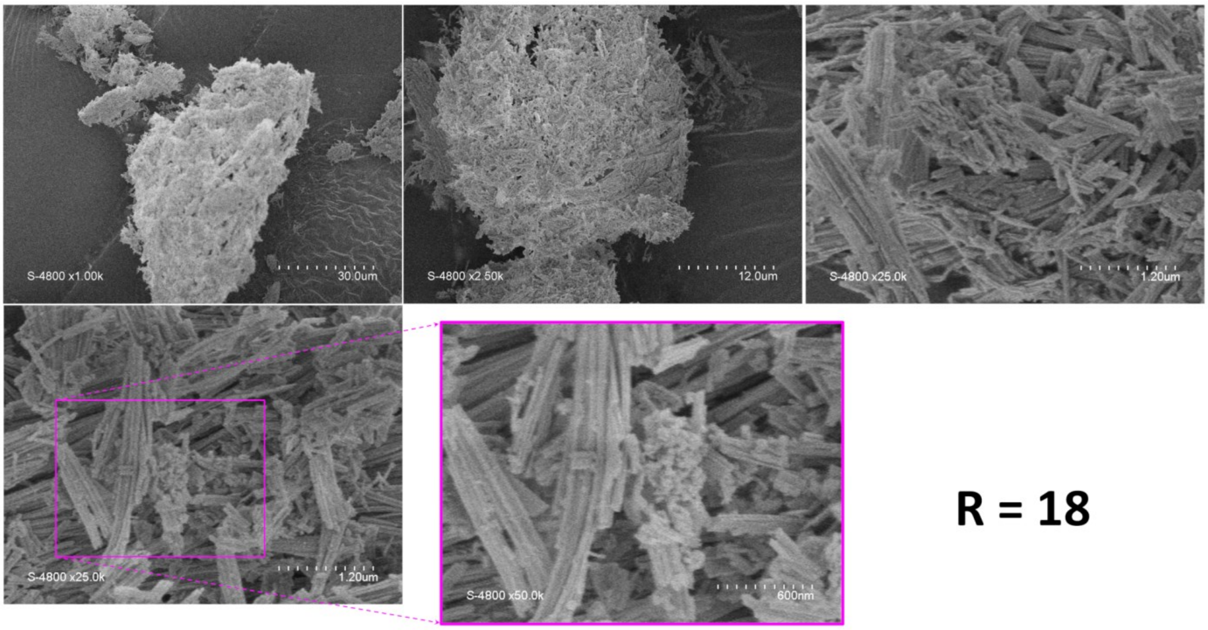

Fig. S6. SEM images of the as-synthesized bismuth-based material for ratio *R* = $n(\mathrm{NaOH})/n(\mathrm{Bi(NO_3)_3 \cdot 5H_2O})$ = 18.

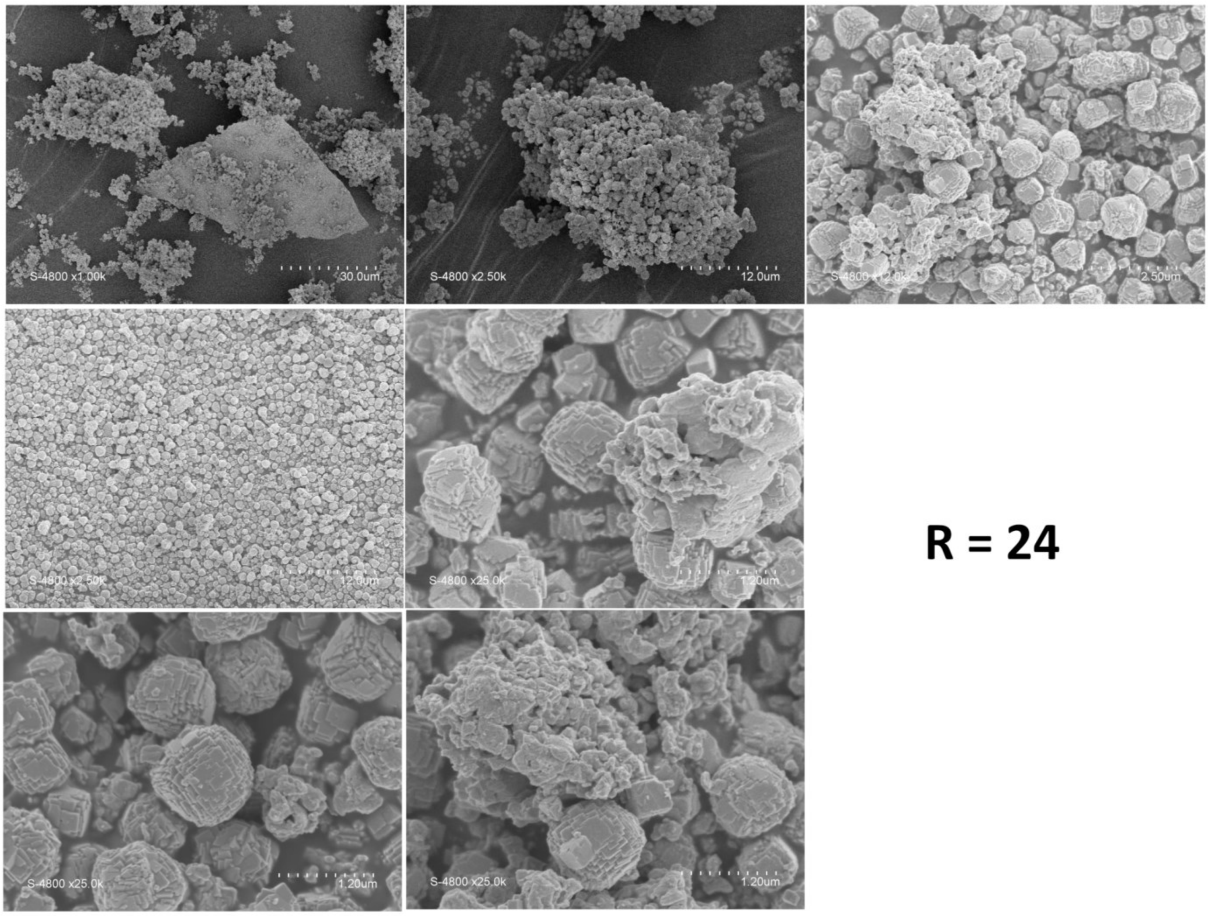

Fig. S7. SEM images of the as-synthesized bismuth-based material for ratio $R = n(\mathrm{NaOH})/n(\mathrm{Bi(NO_3)_3{\cdot}5H_2O}) = 24$.

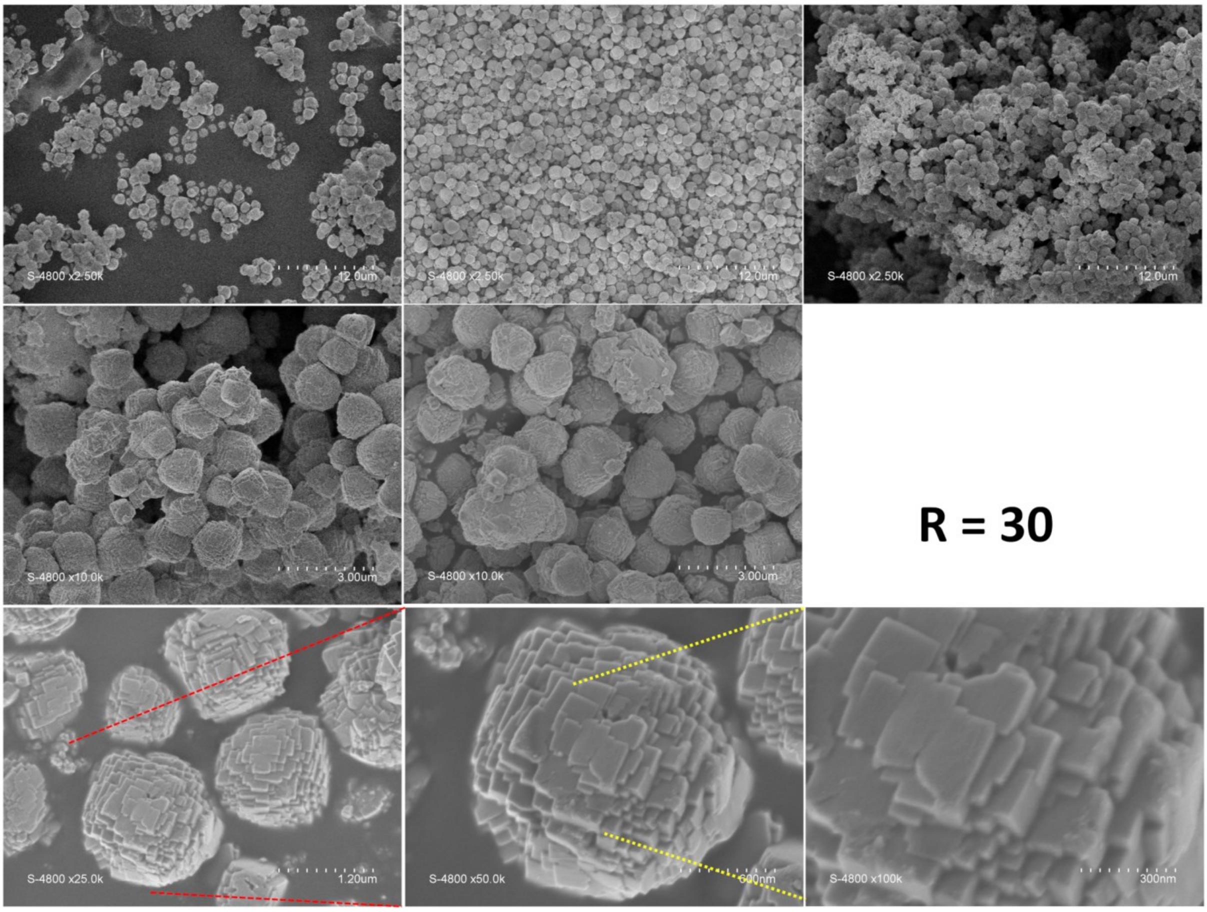

Fig. S8. SEM images of the as-synthesized bismuth-based material for ratio $R = n(\mathrm{NaOH})/n(\mathrm{Bi(NO_3)_3{\cdot}5H_2O}) = 30$.

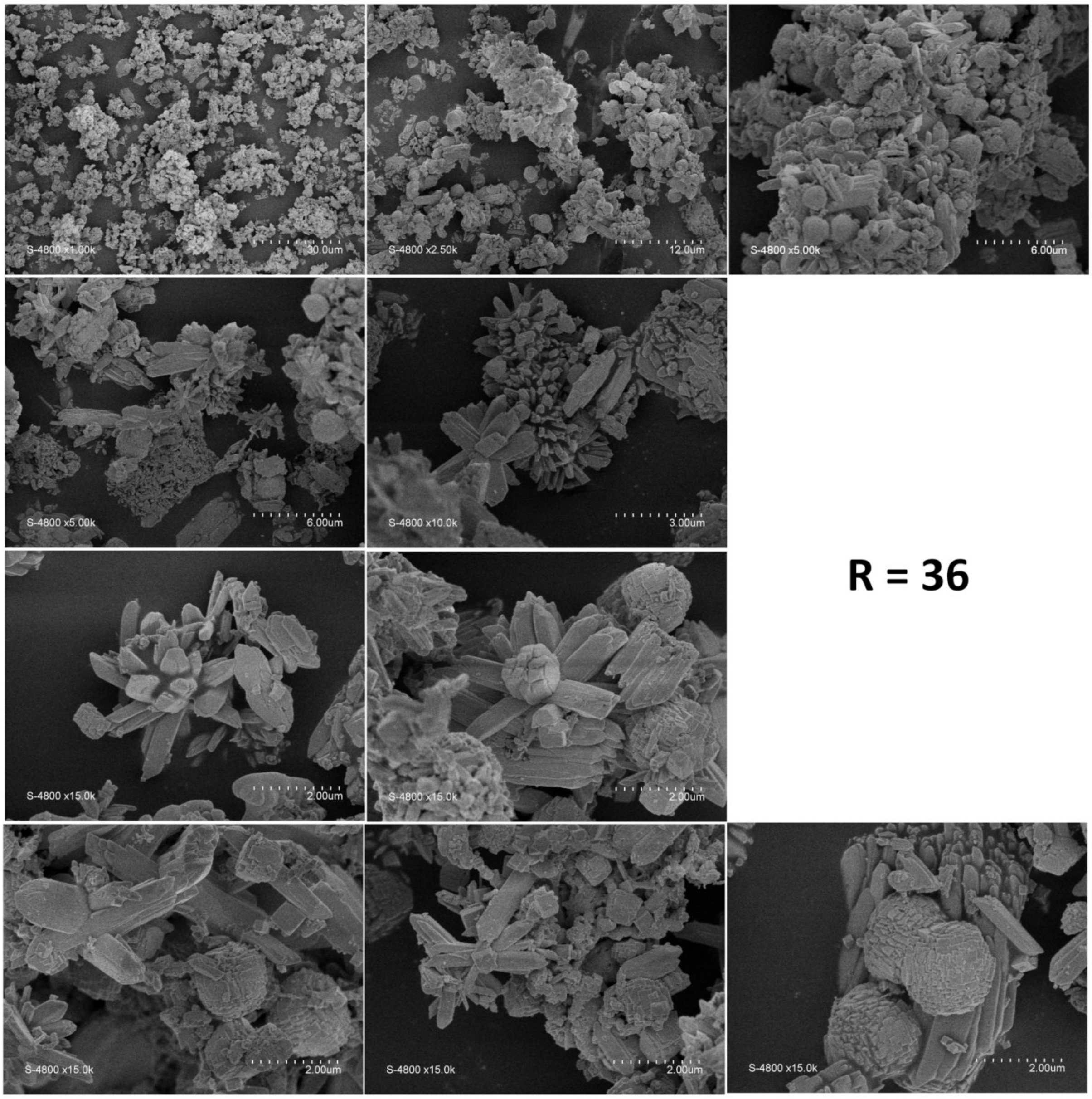

Fig. S9. SEM images of the as-synthesized bismuth-based material for ratio *R* = $n(NaOH)/n(Bi(NO_3)_3 \cdot 5H_2O) = 36$.

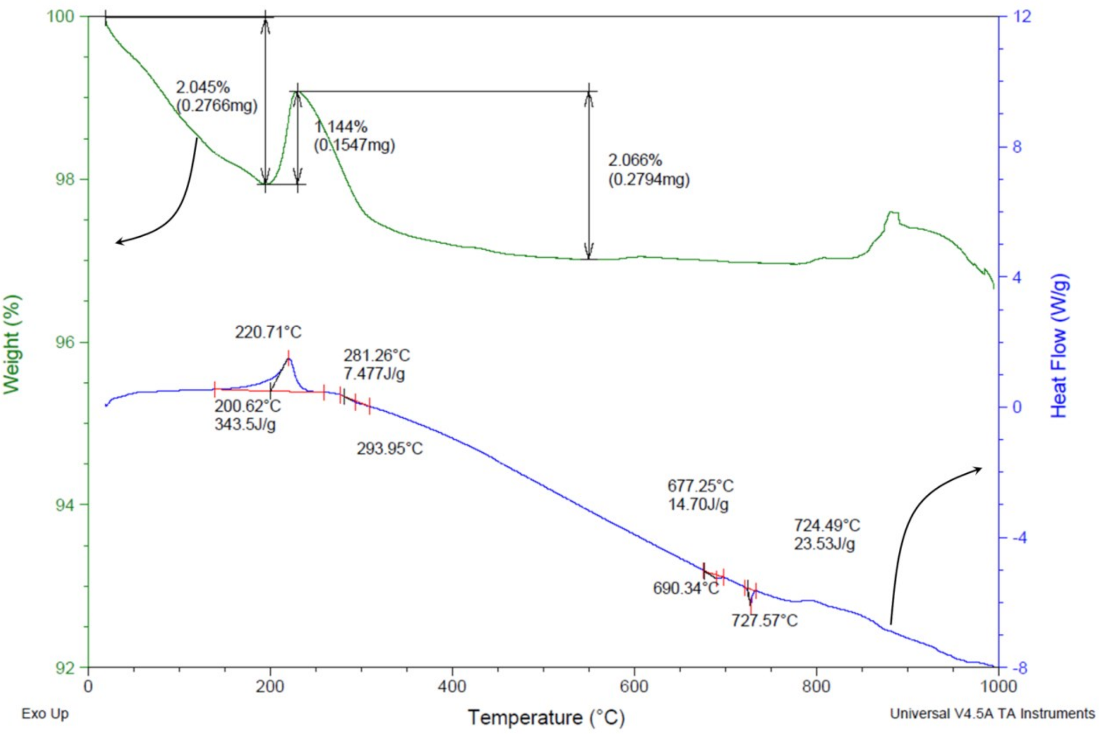

Fig. S10. TGA-DSC of the as-synthesized material for *R* = *n*(NaOH)/*n*($Bi(NO_3)_3 \cdot 5H_2O$) = 30.

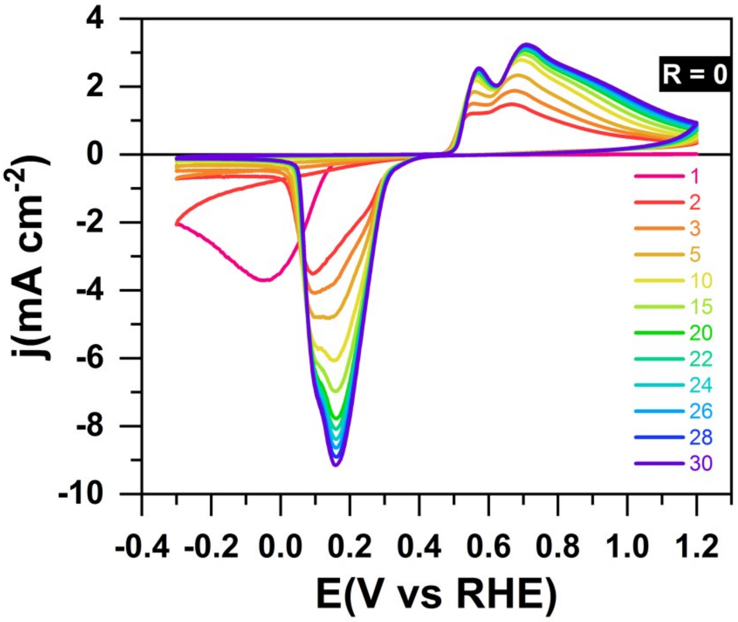

Fig. S11. Material obtained for molar ratio $R = n(\mathrm{NaOH})/n(\mathrm{Bi(NO_3)_3 \cdot 5H_2O}) = 0$. Successive CVs recorded at 100 mV s^{-1} in Ar-saturated 0.1 M KOH.

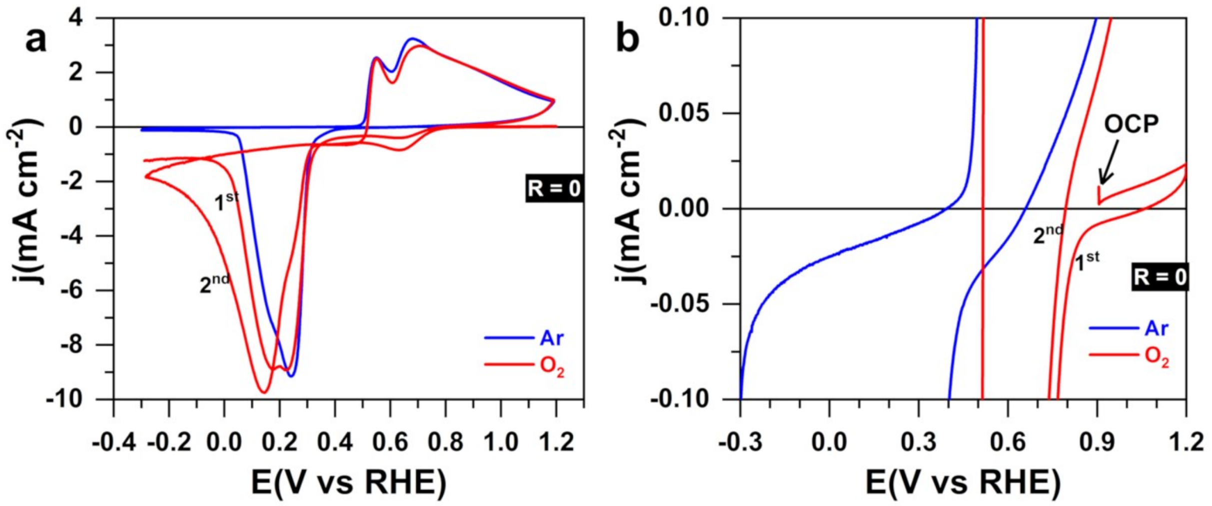

Fig. S12. Material obtained for molar ratio *R* = *n*(NaOH)/*n*($Bi(NO_3)_3·5H_2O$) = 0. (a) CVs at 100 mV s^{-1} in 0.1 M KOH in the presence of Ar (bleu curve, 30th cycle) and in O_2 (red curves: 1st and 2nd cycle). (b) Zoom of the panel (a) showing the starting for CV in the presence of O_2 (after saturation for 20 min: see Fig. 7a in the main text).

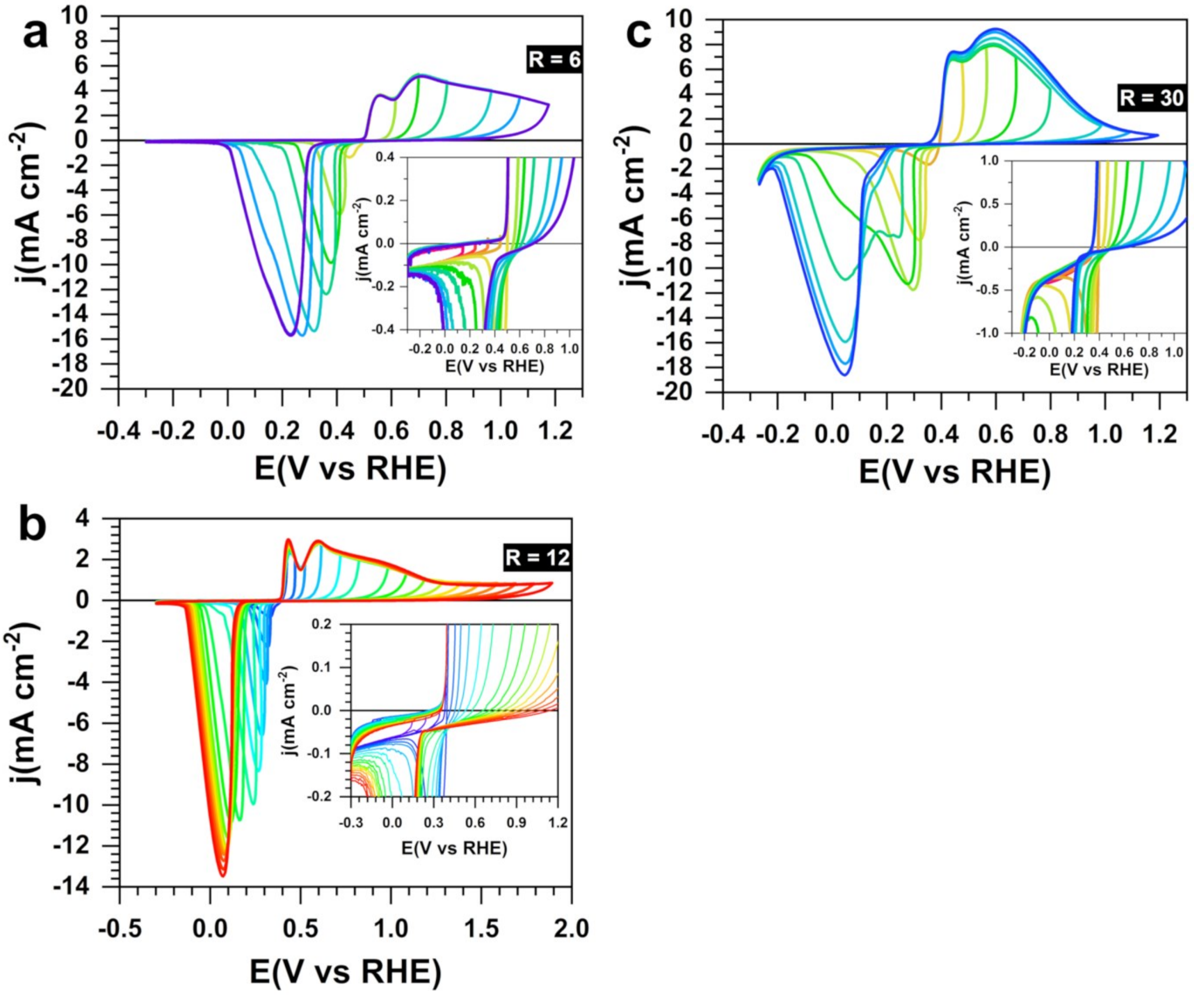

Fig. S13. Materials obtained for molar ratio $R = n(\mathrm{NaOH})/n(\mathrm{Bi(NO_3)_3 \cdot 5H_2O}) = 0$.

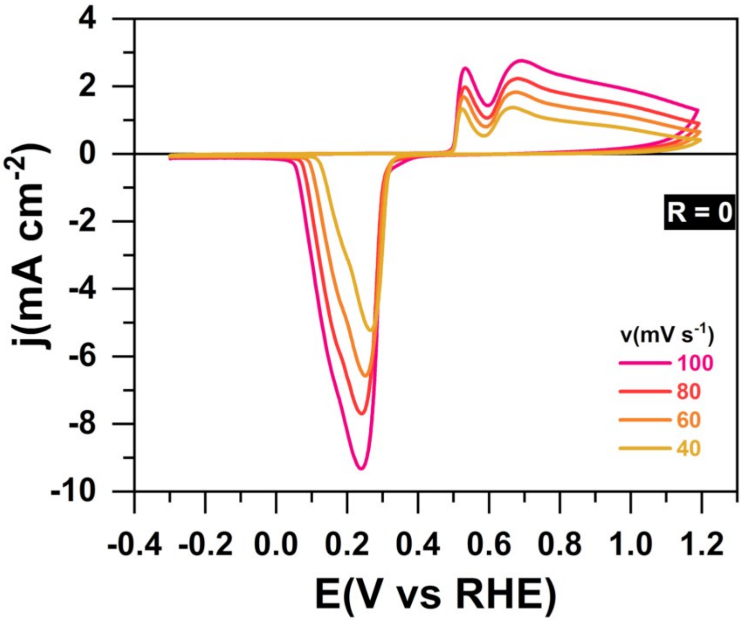

Fig. S14. Materials obtained for molar ratio *R* = *n*(NaOH)/*n*($Bi(NO_3)_3 \cdot 5H_2O$) = 0. Scan rate effect of the CVs collected at 100 mV s^{-1} in Ar-saturated 0.1 M KOH.

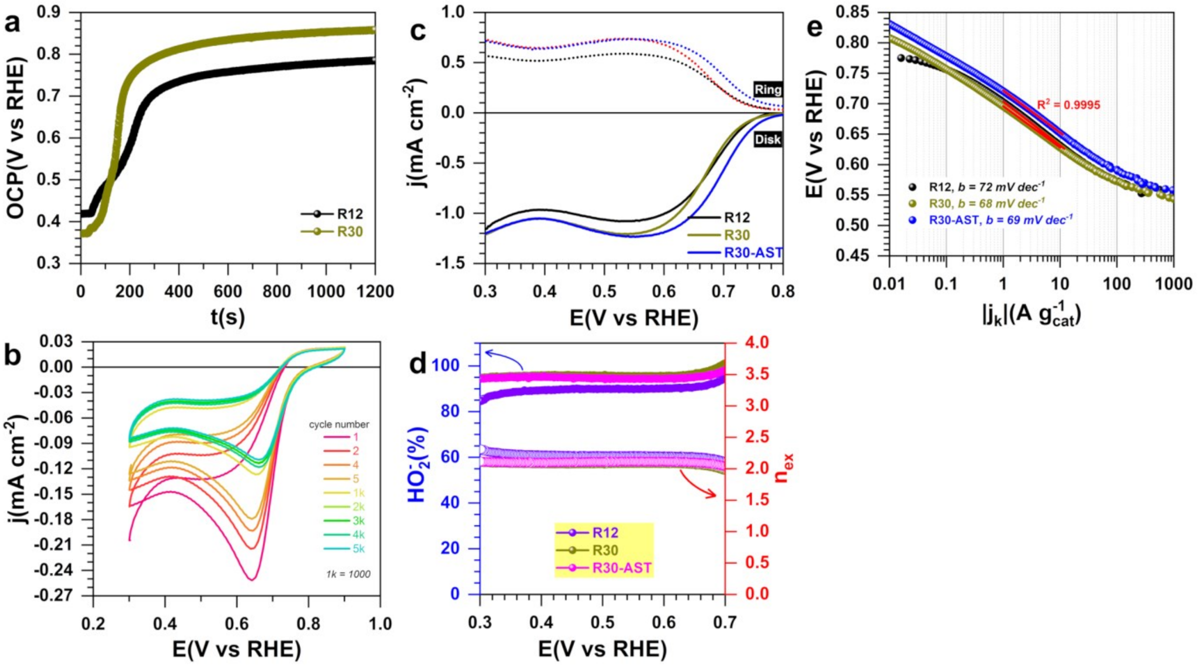

Fig. S15. ORR in 1 M KOH for the materials obtained at different molar ratio: *R* = *n*(NaOH)/*n*($Bi(NO_3)_3 \cdot 5H_2O$). (a) OCP vs time. (b) CVs (iR-uncorrected) recorded at 100 mV s^{-1} during AST for the material obtained for R30. (c) LSV curves recorded from a RRDE setup at 5 mV s^{-1} for the ring (top, normalized by the geometry surface area of the ring (0.11 cm^2)) and disk (bottom, normalized by the geometric surface are of the disk (0.196 cm^2)): the rink was set at 1.2 V vs RHE. (d) Quantitative results in terms of HO_2^- (left *y*-axis) and transferred number of electrons (right *y*-axis). (e) Tafel plots by the kinetic current density normalized by the catalyst loading.

Table S1. EIS results of the as-synthesized bismuth-based materials at different molar ratio: *R* = *n*(NaOH)/*n*($Bi(NO_3)_3 \cdot 5H_2O$) in 0.1 M KOH saturated with O_2. Data were fitted from the equivalent electrical circuit $R_\Omega + Q_{CPE}//R_{ct}$ on Nova 2.1.4 software (Metrohm, Netherlands). EE = Estimated Error (%). The electrode surface was 0.196 cm^2.

Entry	Applied potential E_{appl}(V vs RHE)	Ohmic resistance $R_\Omega(\Omega)$		Charge transfer resistance $R_{ct}(\Omega)$		constant phase element			
						Q_{CPE}(μF $s^{(a-1)}$)		a	
		Value	EE(%)	Value	EE(%)	Value	EE(%)	Value	EE(%)
R = 0	0.672	45.6	0.7	5207.5	1.3	12.9	2.0	0.8	0.4
	0.652	45.5	0.7	3256.8	1.1	12.9	2.3	0.8	0.4
	0.622	46.1	0.8	2052.0	1.3	17.1	3.1	0.8	0.6
R = 6	0.672	42.7	0.7	3111.3	1.2	24.5	2.1	0.8	0.4
	0.652	42.1	0.9	2019.8	1.4	19.9	3.1	0.8	0.6
	0.622	42.1	1.2	1257.1	1.5	18.7	5.9	0.8	1.0
R = 12	0.672	51.9	0.9	2417.3	2.0	18.3	3.2	0.8	0.6
	0.652	52.0	0.8	1866.1	1.7	17.4	3.2	0.8	0.6
	0.622	51.8	0.9	1538.9	1.9	18.5	3.8	0.8	0.7
R = 24	0.672	52.4	0.8	4123.9	2.1	45.8	2.2	0.9	0.5
	0.652	52.4	0.7	3414.9	1.8	43.7	2.2	0.9	0.5
	0.622	52.3	0.6	2413.6	1.6	43.0	2.4	0.9	0.5
R = 30	0.672	50.3	0.9	3917.2	2.0	11.5	2.8	0.9	0.5
	0.652	50.3	0.9	2512.2	1.7	12.0	3.3	0.9	0.6
	0.622	50.2	1.05	1815.1	1.9	12.8	4.1	0.9	0.7

Table S2. Summary of reported electrocatalysts for hydrogen peroxide production in aqueous electrolyte. FE = faradaic efficiency. n.d. = note determined.

Ref	Experimental Conditions	Electroanalytical by RRDE			Productivity by Analytical methods after electrolysis		
		Selectivity (%)	n_{ex}	j_k(A g^{-1})	mol kg^{-1}_{cat} cm^{-2}	mol kg^{-1}_{cat} h^{-1}	FE (%)
Herein	Bismuth-based materials (sample R30) in 1 M KOH	96	2.1	30 (at 0.6 V vs RHE) 930 (at 0.55 V vs RHE)	69	138	92
Chang, Q. et al.[3] Nat. Commun. 2020, 11, 2178.	$Pd^{\delta+}$-OCNT in 0.1 M $HClO_4$	95	n.d.	597 (at 0.55 V vs RHE)		1701	87
Xia, C. et al.[4] Science 2019, 366, 226-231.	Carbon black in 1 M Na_2SO_4 (pH7)	98	n.d.	n.d.	n.d.	3660	90-95
San Roman, D. et al.[5] ACS Catal. 2020, 10, 1993-2008.	nanowire-templated out-of-plane three-dimensional fuzzy graphene (NT-3DFG) in 0.1 M KOH	n.d.	2.5-3	n.d.	n.d.	n.d.	94
Ledendecker, M. et al.[6] ACS Catal. 2020, 5928-5938.	PdClx/C in 0.1 $HClO_4$	90	n.d.	73 (potential not specified)	n.d.	n.d.	n.d.
Sun, Y. et al. [7] ACS Catal. 2018, 8, 2844-2856.	Nitrogen-Doped Mesoporous Carbon Catalysts in 0.1 M KOH	85	2.1	n.d.	n.d.	562	70
Zakaria, M. B. et al.[8] J. Mater. Chem. A 2016, 4, 9266-9274.	Mn-Ru oxide in 0.1 M NaOH	100	2.0	n.d.	n.d.	n.d.	n.d.
Kim, H. W. et al.[9] Nature Catalysis 2018, 1, 282-290.	mild reduction of graphene oxide (mrGO) in 0.1 M KOH	100	2.0	110 (at 0.6 V vs RHE)	n.d.	n.d.	n.d.

Note for up-to-date data in May 2020: Readers are suggested to refer to Table 1 of a recent Perspective:[10] Jung, E.; Shin, H.; Hooch Antink, W.; Sung, Y.-E.; Hyeon, T., “Recent Advances in Electrochemical Oxygen Reduction to H_2O_2: Catalyst and Cell Design. ACS Energy Lett. 2020, DOI: 10.1021/acsenergylett.0c00812, 1881-1892”. Publication Date: May 8, 2020. https://doi.org/10.1021/acsenergylett.0c00812.

References

1. E. Gileadi, *Electrods Kinetics for Chemists, Chemical Engineers, and Materials Scientists*, Wiley-VCH, New York, N Y, USA, 1993.
2. T. W. Napporn, Y. Holade, B. Kokoh, S. Mitsushima, K. Mayer, B. Eichberger and V. Hacker, in *Fuel Cells and Hydrogen: From Fundamentals to Applied Research*, eds. V. Hacker and S. Mitsushima, Elsevier, 2018, DOI: 10.1016/B978-0-12-811459-9.00009-8, pp. 175-214.
3. Q. Chang, P. Zhang, A. H. B. Mostaghimi, X. Zhao, S. R. Denny, J. H. Lee, H. Gao, Y. Zhang, H. L. Xin, S. Siahrostami, J. G. Chen and Z. Chen, *Nat. Commun.*, 2020, **11**, 2178.
4. C. Xia, Y. Xia, P. Zhu, L. Fan and H. Wang, *Science*, 2019, **366**, 226-231.
5. D. San Roman, D. Krishnamurthy, R. Garg, H. Hafiz, M. Lamparski, N. T. Nuhfer, V. Meunier, V. Viswanathan and T. Cohen-Karni, *ACS Catal.*, 2020, **10**, 1993-2008.
6. M. Ledendecker, E. Pizzutilo, G. Malta, G. V. Fortunato, K. J. J. Mayrhofer, G. J. Hutchings and S. J. Freakley, *ACS Catal.*, 2020, **10**, 5928-5938.
7. Y. Sun, I. Sinev, W. Ju, A. Bergmann, S. Dresp, S. Kühl, C. Spöri, H. Schmies, H. Wang, D. Bernsmeier, B. Paul, R. Schmack, R. Kraehnert, B. Roldan Cuenya and P. Strasser, *ACS Catal.*, 2018, **8**, 2844-2856.
8. M. B. Zakaria, C. Li, M. Pramanik, Y. Tsujimoto, M. Hu, V. Malgras, S. Tominaka and Y. Yamauchi, *J. Mater. Chem. A*, 2016, **4**, 9266-9274.
9. H. W. Kim, M. B. Ross, N. Kornienko, L. Zhang, J. Guo, P. Yang and B. D. McCloskey, *Nat. Catal.*, 2018, **1**, 282-290.
10. E. Jung, H. Shin, W. Hooch Antink, Y.-E. Sung and T. Hyeon, *ACS Energy Lett.*, 2020, **5**, 1881-1892.